

# Sclera boundary localization using circular hough transform and a modified run-data based algorithm

Tunde Taiwo Adeniyi<sup>1</sup>, Oladele Tinuke Omolewa<sup>1</sup>, Jide Kehinde Adeniyi<sup>2</sup>

<sup>1</sup>Department of Computer Science, University of Ilorin, Ilorin, Nigeria

<sup>2</sup>Department of Computer Science, College of Pure and Applied Sciences, Landmark University, Omu-aran, Nigeria

## Article Info

### Article history:

Received Sep 29, 2022

Revised Feb 2, 2024

Accepted Feb 13, 2024

### Keywords:

Biometrics

Circular hough transform

Compound local binary pattern

Modified run-data algorithm

Sclera boundary localization

## ABSTRACT

Security challenges over the years has led to the need for an improvement in the traditional security approaches. This led to the advent of biometrics. Recently, among the biometric approaches, sclera has been an area of immense study. This is due to its accuracy; however, segmentation of the sclera has been a limiting factor to the application of this biometric trait. Several approaches have been proposed in literature but there is still the need to improve the segmentation accuracy. This study proposes the use of circular hough transform and a modified run-data based algorithm. The study also presented a sclera recognition system using the compound local binary pattern for features extraction and Manhattan distance for classification. The system produced a segmentation accuracy of 99.9% for sclera blood vessels, periocular and iris (SBVPI) sclera database and 100% for manually captured sclera database. The system produced an accuracy of 99.98 for SBVPI sclera database and 99.99% for manually captured sclera database.

*This is an open access article under the [CC BY-SA](https://creativecommons.org/licenses/by-sa/4.0/) license.*



## Corresponding Author:

Jide Kehinde Adeniyi

Department of Computer Science, College of Pure and Applied Sciences, Landmark University

Omu-aran, Nigeria

Email: adeniyi.jide@lmu.edu.ng

## 1. INTRODUCTION

The increase in the growth of digital technology has led to the need for better security methods. This led to the increase in the application of biometric technology in identity verification and authentication. This increase is due to the reliability and unique nature of biometric traits. Biometric authentication uses a person's behavioural or physical trait for recognition [1], [2]. These traits include iris, fingerprint, palmprint, iris, signature, and among other [2], [3]. These traits can be categorized as being physical or behavioural. The physical trait answers the question of who an individual is, while the behavioural trait answers how an individual does something. Among the physical trait are those that are related to an individual's ocular properties (that is the iris, pupil, and sclera) [1], [3].

The iris is noted for its accuracy in near infrared images; however, this drops in visible light wavelength with no constraint during capturing [4]. To alleviate the challenges associated with both traits, pairing the trait with another would improve the performance of iris [5], [6]. This is termed multimodal biometrics; the use of more than one biometric trait for recognition. This is usually aimed at increasing accuracy and increasing the difficulty of tricking the system. Among the other suitable biometric traits that can be combined with iris, sclera seems to be most suitable [6], [7]. This is because it can be captured with the iris. Iris is the outer circle of the human eye, while the sclera is the white part of the eye.

Sclera trait is an area of biometric that has recently been receiving attention and this is due to the fact that it is a highly-protected part of the eye that is difficult to forge. The vessel pattern on the sclera is studied and found to not be the same for two people and different for two pairs of eyes [8], [9]. This uniqueness makes it suitable for use as a biometric trait and there is a need to develop an efficient recognition system for the trait. However, the segmentation of the sclera from the eye image has limited the application of this biometric trait. Several studies have proposed different approaches for sclera segmentation; however, the segmentation accuracy shows that there is still a lot of room for improvement [10], [11]. Hence, this study examines the segmentation of sclera from the eye image. It also presents a sclera recognition system.

## 2. RELATED WORKS

Sclera trait in biometric is important in biometric as it can uniquely identify an individual. It can further be combined with other ocular biometrics to increase the accuracy of the system. Recent trends have examined the segmentation of sclera in the eye image and use of this biometric trait for recognition in a unimodal and multimodal way. Literatures relevant to both sclera segmentation and recognition in this section.

### 2.1. Sclera segmentation

Rot *et al.* [1] developed a cascaded convolutional neural network (CNN) assembly for segmenting sclera. They went further to propose a CNN model (ScleraNet) for extraction of discriminatory features from the sclera. A new sclera dataset of ocular images named sclera blood vessels, periocular and iris (SBVPI) was collected. An accuracy of 93.3% was recorded. In the study by Xu *et al.* [2], they proposed a model for sclera segmentation. It starts with filtering using median filter. The Cr colour channel image. Saviola method for iris segmentation. Global otsu algorithm and adaptive otsu algorithm were applied to the two segmented images and the output was fused together. the local area histogram equalization was used for image enhancement. The length of blood vessels was used for discrimination. They recorded a segmentation accuracy of 98.1%.

Pathak *et al.* [3] also proposed sclera segmentation system. Their system starts with preprocessing, using bilateral filtering. After this, features were extracted in the form of brightness, colour and texture. Using the extracted features, CNN was used for the segmentation of the sclera, iris and pupil based on the entropy value. An accuracy of 98% and 99.423 was obtained on Multimedia University (MMU) and Universidade de Beira Iris (UBIRIS) v.2 datasets respectively.

Maheshan *et al.* [4] proposed the segmentation of sclera from the eye image using a modified intuitionistic fuzzy clustering approach. This is aimed at improving the performance of the traditional fuzzy set that non-membership value is always the complement of the membership value. They obtained a precision of 85.10 and a recall of 77.90. In the study by Vitek *et al.* [5], sclera segmentation was performed using a region growing method called Active contour without edge. In their approach, two points are initialized, after which the active contour without edge is performed.

### 2.2. Sclera recognition

Among the recent study in sclera recognition is the work of Pathak *et al.* [6]. The paper presented a multimodal biometrics recognition using the pupil, iris and sclera. The preprocessing starts with the use of min-max normalization. After which entropy based CNN was used to segment the image. The colour histogram features, gabor features and Y-shaped features were used to calculate the support value of each trait respectively. UBIRIS V2 database was used for testing the system. An accuracy of 97.99% was recorded.

In the study by Maheshian *et al.* [7], they explored the use of deep learning for sclera recognition. In particular they proposed a custom layer CNN that they termed CNN sclera recognition engine (CNSRE). The network model is made up of four convolutional units and a fully connected layer. An accuracy of 87.65 was recorded.

Lee and Kim [8] proposed a sclera recognition system using bifurcation-based descriptor. The sclera was segmented from the ocular image, and the blood vessels were extracted. Morphological operation was used to thin the blood vessels extracted. The bifurcation of the blood vessels was extracted and the distance between the central bifurcation and its neighbours were used as features. Each local structure is then matched. The result showed an equal error rate (EER) of 1.92%.

The study by Zhu *et al.* [9] proposed a sclera recognition method that consist of a non-learning based segmentation method and a supervised learning technique for classification. Contrast limited adaptive histogram equalization (CLAHE) was applied to segment the sclera from the eye image. Their approach introduced a stem-and-leaf branches network for classification. A new sclera dataset named ScleraVO was introduced. Their system showed an accuracy of 96.91.

### 3. METHOD

The block diagram of the system is shown in the Figure 1. This details the key operations to be performed by the system. It includes collection of eye images, filtering of each eye image, segmentation, features extraction, and matching.

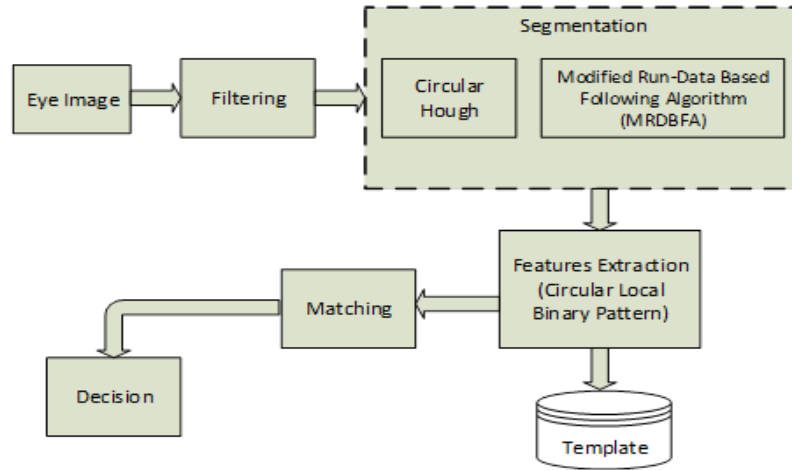


Figure 1. Block diagram of the designed system

#### 3.1. Eye image

For this system, the SBVPI eye database and manually captured eye images were used [1]. For the SBVPI database, 1000 eye images were used for testing. 500 eye images were genuine and the remaining half not genuine (not registered on the system). For the manually capture eye images, a canon EOS 60D camera was used to capture 200 eye images. Both eye image dataset was used in the developed system. A sample SBVPI eye image is shown in Figure 2.



Figure 2. A sample eye image

#### 3.2. Grayscale conversion

This involves representing the image in its gradient form. Computing the average of the red, green, and blue value for each pixel gives the gradient form of the image. Figure 3 shows the grey output of Figure 2.



Figure 3. Gray eye image output

### 3.3. Canny edge detection

Canny edge detection algorithm is used to convert the image to a binary form which depicts the edges of the image. It consists of the following steps [10], [11].

#### 3.3.1. Filtering

Filtering is aimed at reducing noise and unwanted textures in the ocular image. In (1) and (2) shows the image  $f(m, n)$  filtered into  $g(m, n)$ .

$$g(m, n) = G_{\sigma}(m, n) * f(m, n) \quad (1)$$

where

$$G_{\sigma}(m, n) = 1/\sqrt{(2\pi\sigma)^2} \exp(-(m^2 + n^2)/(2\sigma)^2) \quad (2)$$

$f(m, n)$  represents the image.

Where  $m$  is the distance in the horizontal axis,  $n$  is the distance in the vertical axis, and  $\sigma$  is the standard deviation of the Gaussian distribution [12].

#### 3.3.2. Finding the gradient

The gradient measure on the image is performed with the sobel operator. The edge detection operator (sobel) returns a value for the first derivative in the horizontal direction ( $g_m$ ) and the vertical direction ( $g_n$ ). From this the edge gradient and direction can be obtained using (3) [13].

$$M(m, n) = \sqrt{(g_m)^2(m, n) + (g_n)^2(m, n)} \quad (3)$$

The sobel operator estimates gradient in the  $m$  and  $n$  direction using two convolutional masks. The masks are shown in Figure 4. The  $g_m$  estimates gradient in the  $m$  direction and the  $g_n$  estimates gradient in the  $n$  direction.

1	2	1
0	0	0
-1	-2	-1

$g_m$

-1	0	1
-2	0	2
-1	0	1

$g_n$

Figure 4. Two tables showing sobel masks (kernel),  $g_m$  and  $g_n$  respectively

Where the direction of the edge was computed with (4) using the gradient in the  $m$  and  $n$  direction,

$$\theta(m, n) = \tan^{-1} [g_n(m, n)/g_m(m, n)] \quad (4)$$

#### 3.3.3. Edge direction

After determining the edge direction, the obtained edge direction is then converted to a direction that can be traced in the image [14]. The possible direction that can be traced can one of the eight neighbouring pixels. The eight directions are north, north-east, north-west, right, left, south, south-east and south-west of the pixel being considered.

#### 3.3.4. Suppress non-maxima pixels

After the direction of the edges are gotten, non-maximal suppression is performed on the image. To trace along the edges and set to zero pixels not considered edges, non-maximal suppression was used. The output of this step is a thinned edge line [15].

#### 3.3.5. Double thresholding

Two thresholds were chosen as  $T_1$  and  $T_2$  (that is  $T_2$  is the major edge and  $T_1$  is a minor edge) such that ( $T_1 < T_2$ ) to obtain the binary image. Edge segments of  $T_2$  were linked to obtain the continuous edges and any that was below  $T_2$  and was greater than  $T_1$  that lies along the continuous  $T_2$  edge segments was consider a major edge [16].

### 3.3.6. Linking of edges

The final step involves linking the edge segments to form continuous edges [11], [14], [15]. Edge image from canny edge detection algorithm as shown in Figure 5. Figure 5 shows the edge image of Figures 2 and 3.

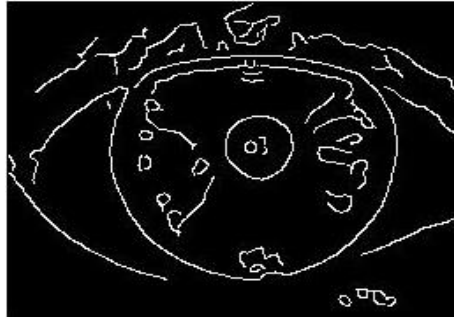


Figure 5. Edge image from canny edge detection algorithm

### 3.4. Circular hough transform

Circular hough transform is used to detect the iris boundary and the pupil boundary. The output of this gives the center coordinates of the iris and the pupil [3], [17], [18]. It also gives the radius of the iris and the pupil. The CHT is represented in (5) [12], [19]. Figure 6 shows the pupil boundary detected after using the hough transform on Figure 5.

$$\|(x - a)\|^2 + \|(y - b)\|^2 = r^2 \quad (5)$$

With  $a$  and  $b$  being the center of the circle in  $x$  and  $y$  directions respectively and  $r$  being the radius. The parameter of the circle is as shown in (6) and (7) [20]–[22].

$$x = a + r\cos(\theta) \quad (6)$$

$$y = b + r\sin(\theta) \quad (7)$$

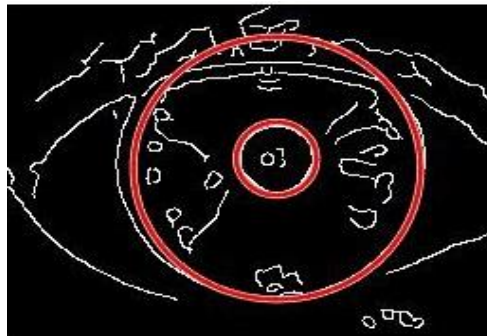


Figure 6. Pupil boundary detection using circular hough transform

### 3.5. Segmentation using the modified run-data-based following algorithm

The traditional edge-point tracing of run data is used in the run-data-based following method, which employs run data in pairs consisting of an object's left and right edges that are produced using horizontal scan lines from left to right on an image. There may be an outer contour and multiple inside contours on the object. There are five types of run data: left edge of outer contour, right edge of outer contour; left edge of inner contour, right edge of inner contour; left edge of inner contour; right edge of inner contour.

inner contour, left edge of inner contour; right edge of inner contour, right edge of outer contour; right edge of inner contour, right edge of outer contour; and right edge of outer contour, left edge of outer contour [23].

However, for extraction of sclera, modifications were proposed to the traditional run-data-based algorithm. The modified run-data-based following algorithm was applied after the detection of the iris boundary. The key-points were located using the center co-ordinates of the iris boundary and the radius of the iris that were detected. The key-points detected are the eight points at the right sclera and the left sclera. These points helped in cropping out two images from the left and right sclera. To locate the points, a modified run-data-based following (MRDBF) algorithm was used. It must be noted that the MRDBF algorithm does not directly trace the boundary but picks points (8 points) that forms two rectangular boundaries within the sclera regions (right and left) as shown in Figure 7. The changes made to the algorithm include: the starting point for the algorithm is dependent on the circular hough transform. Also, the tracing is done within the boundary of the image with the purpose of locating distinct and consistent points within the boundary and this is helpful in the case where the boundary is not completely defined. As opposed to scanning the image row-wise and column-wise to detect the inner and outer pixels, the algorithm scans the image from the reference points. The MRDBF algorithm is shown in Algorithm 1.

Figure 8 shows the flow chart of the proposed algorithm. The points detected in Figure 7 are shown in Figure 9. Using the eight key-points (P1-P8), the sclera is cropped out. Figure 10(a) shows the sclera image cropped out using eight key-points on the left side of the iris. Figure 10(b) shows the sclera image cropped out using eight key-points on the right side of the iris.

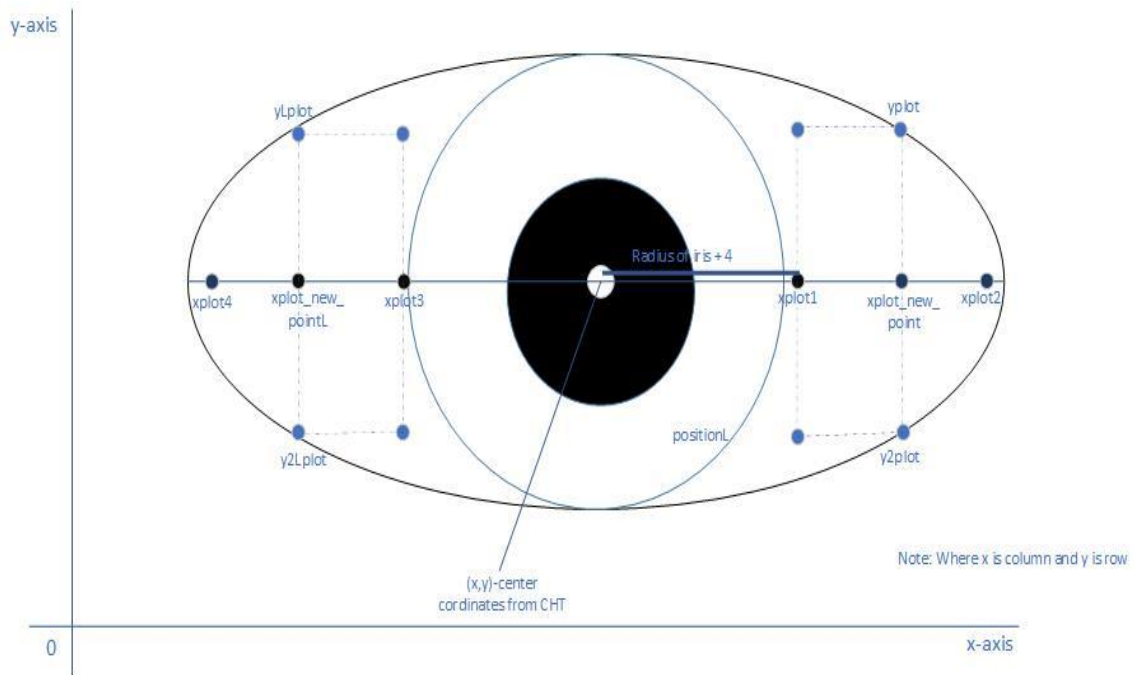


Figure 7. Modified run-data-based following algorithm

Algorithm 1: Modified Run-Data-Based Following Algorithm

**Input:** An array of binary pixels of an eye image ( $P$ ) with  $P = \{0,1\}$ . Where 0 is the background pixel and 1 is an edge pixel.

Let  $m$  and  $n$  be the dimension of the input array respectively.

Let  $CHT\_row$  and  $CHT\_col$  be the row and column center co-ordinate of the iris returned by the CHT (Circular Hough transform)

Let  $Iris\_r$  be the radius of the iris.

**Start:**

1.  $xplot1 = CHT\_col + Iris\_r + 4$
2.  $yplot1 = CHT\_row$
3. for  $b = xplot1:1:n$  (i.e. increment by 1 and stop at end of column)
  - if  $P(yplot1, b) = 1$  (i.e. checking for foreground)
    - $xplot2 = b$  (i.e. detect the column point for  $xplot2$  (length of the sclera region))
  - break

```

        else
            xplot2 = n
        end if
    end

4. xplot3 = CHT_col - Iris_r - 4
5. yplot3 = CHT_row
6. for b = xplot3: -1: 1 (i.e decrementing by 1)
    if P (yplot3, b) == 1 (i.e. checking for foreground)
        xplot4 = b
        break
    else
        xplot4 == 1
    end if
end

//Detecting points for the first rectangle
7. xplot_new_poin = (xplot2- xplot1)/ 2
8. xplot_new_point = (xplot1 + xplot_new_point) (i.e. getting a point between xplot1
and xplot 2 for a rectangle)
9. yplot_new_point = yplot1
10. for y=yplot_new_point: 1: m (i.e. incrementing by 1 to the end of row)
    if P (y, xplot_new_point) == 1
        y2plot = y (i.e. new point y2plot)
        break
    end if
end
11. for y = yplot_new_point: -1: 1 (i.e. decrement by -1)
    if P (y, xplot_new_point) == 1
        yplot = y
        break
    else
        end if
end

//points detected are:
//P1(yplot, xplot_new_point)
//P2(y2plot, xplot_new_point)
//and
//P3(yplot, xplot1)
//P4(y2plot, xplot1)
// Detecting points for the left rectangle
12. xplot_new_poinL = (xplot3 - xplot4)/2
13. xplot_new_pointL = (xplot3-xplot_new_point)
14. yplot_new_pointL = yplot3
15. for y = yplot_new_pointL: 1: m
    if P (y, xplot_new_pointL) == 1
        y2Lplot = y (i.e. new point y2Lplot)
        break
    else
        endif
end
16. for y = yplot_new_point: -1: 1
    if P (y, xplot_new_pointL) == 1
        yLplot = y (i.e. new point yLplot)
        break
    else
        end if
end

//points detected are:
//P5(yLplot, xplot_new_pointL)
//P6(y2Lplot, xplot_new_pointL)
//and
//P7(yLplot, xplot3)
//P8(y2Lplot, xplot3)

```

**Output:** The points detected are the points P1, P2, P3, P4, P5, P6, P7, P8 with their respective co-ordinates.

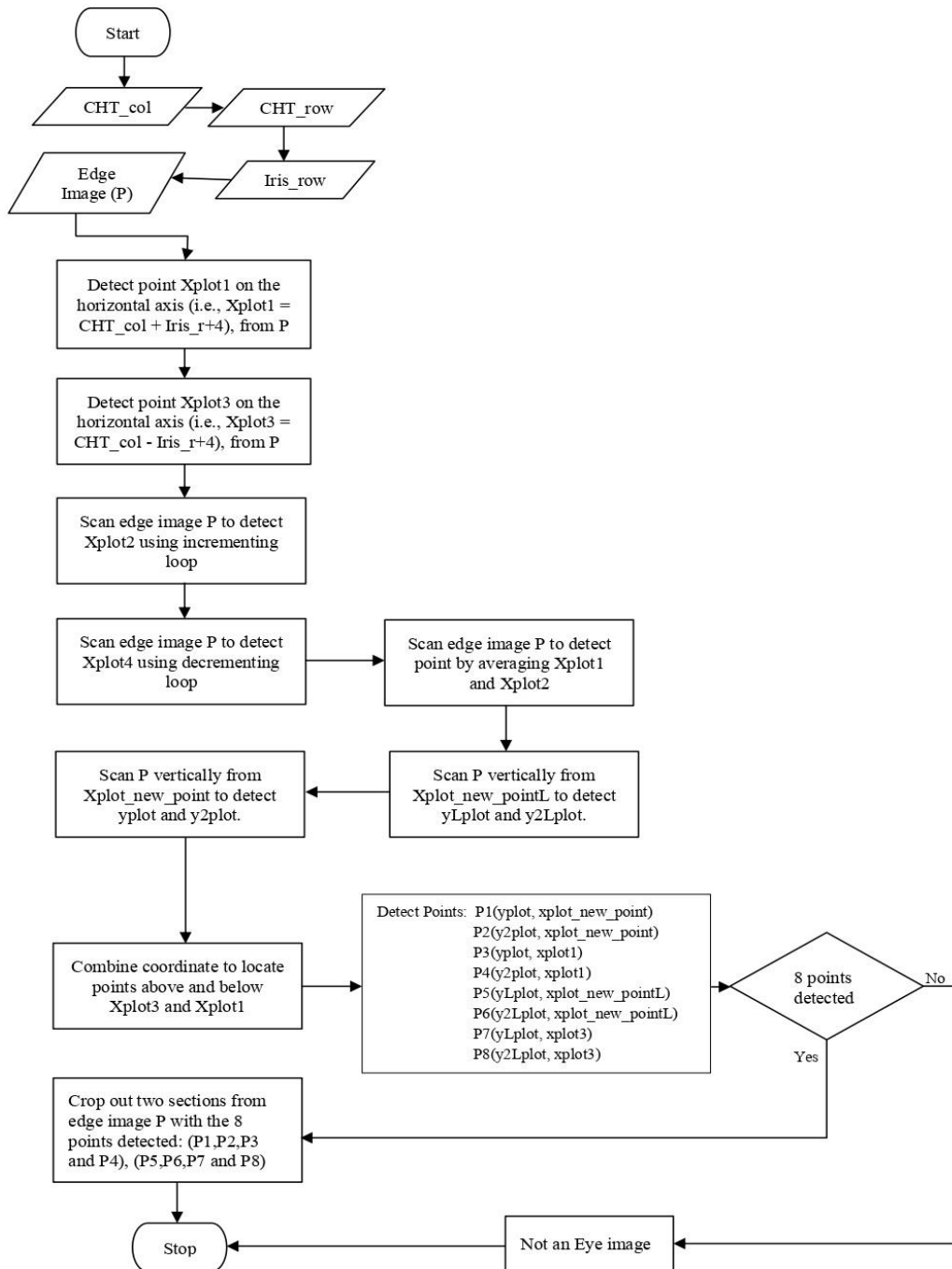


Figure 8. Flowchart of the modified run-data-based following algorithm



Figure 9. Figure showing the eight key-points (P1-P8)



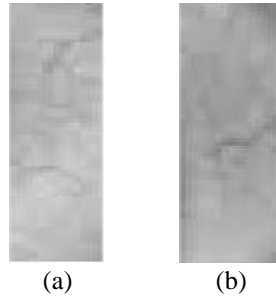


Figure 10. Sclera image extracted from the of the eye image; (a) sclera image of the left side of the iris and (b) sclera image of the right side of the iris

### 3.6. Features extraction

The feature extracted from the sclera image is the gradient of the segmented sclera regions. In terms of the segmented iris image, the gradient (patterns) of the iris was extracted. For the features extraction of the iris and the sclera, compound local binary pattern (CLBP) was used. LBP is known for its computational simplicity and resistance to changes in illumination; however, it discards the magnitude information of the difference between the center and the neighbour gray values in a local neighbourhood. This may result in inconsistent codes which is resolved by CLBP. The equation for CLBP is shown in (8) [24], [25]:

$$s(i_p, i_c) = \begin{cases} 00 & i_p - i_c < 0, \quad |i_p - i_c| \leq M_{avg} \\ 01 & i_p - i_c < 0, \quad |i_p - i_c| > M_{avg} \\ 10 & i_p - i_c \geq 0, \quad |i_p - i_c| \leq M_{avg} \\ 11 & \text{Otherwise} \end{cases} \quad (8)$$

where,  $i_c$  is the grey value of the center pixel,  $i_p$  is the gray value of a neighbour  $p$ , and  $M_{avg}$  is the average magnitude of the difference between  $i_p$  and  $i_c$  in the local neighbourhood. Figure 11 shows the equivalent CLBP of the extracted sclera images after they were joined together.



Figure 11. CLBP of sclera image

### 3.7. Matching

For the matching, Manhattan distance was used. Manhattan distance is the sum of the absolute difference between two vectors in n-dimensional vector space. According to Shang *et al.* [26], it is the sum of the absolute differences of their corresponding components. It is as shown in (9) [27].

$$d(X, Y) = \sum_{i=1}^n |x_i - y_i| \quad (9)$$

### 3.8. Performance evaluation metrics

The evaluation of the developed system was performed using the false acceptance ratio (FAR), the false rejectance ratio (FRR), and the accuracy. The methods were selected because of the frequent use in literature. The FAR is the ratio of falsely accepted users to the total false users tested. The FRR is the ratio of falsely rejected users to the total genuine users submitted. The FAR and FRR are also known as the false positive ratio (FPR) and false negative ratio (FNR) respectively. The accuracy of the system is the percentage of the users that were correctly identified by the biometric system. To compute the FAR and FRR, the true

positive (TP), false negative (FN), false positive (FP), and true negative (TN) are required. The TP is the number of genuine individuals that were positively predicted. The FN is the number of genuine users that are predicted negative. The FP is the number of impostors that were predicted positive. The TN is the number of impostors that were negatively predicted. In (10) to (12) shows the FAR, FRR and accuracy [28], [29].

$$FAR = FPR = FP / (FP + TN) \tag{10}$$

$$FRR = FNR = FN / (TP + FN) \tag{11}$$

$$Accuracy = 100 - \frac{FAR + FRR}{2} \tag{12}$$

**4. RESULTS AND DISCUSSION**

Tables 1 and 2 show the confusion matrix of the manually captured eye images and the SBVPI eye image database. From Tables 1 and 2, (10) and (11), the FAR and FRR obtained after testing the system are both 0.01. This produced an accuracy of 99.99 for the manually captured eye images using the canon camera. The SBVPI database of eye images gave an accuracy of 99.98, with the FAR and FRR being 0.016 and 0.024 respectively. The EER for the system was used to select the optimum threshold for matching. The EER for this system is shown in Figure 12.

Table 1. Confusion matrix of the manually captured eye images

eye images			
Total no=200	Predicted-no	Predicted-yes	
Actual-no	TN=99	FP=1	100
Actual-yes	FN=1	TP=99	100
Total	100	100	200

Table 2. Confusion matrix of SBVPI eye image database

database			
Total no =1000	Predicted-no	Predicted-yes	
Actual-no	TN=488	FP=12	500
Actual-yes	FN=8	TP=492	500
Total	496	504	1000

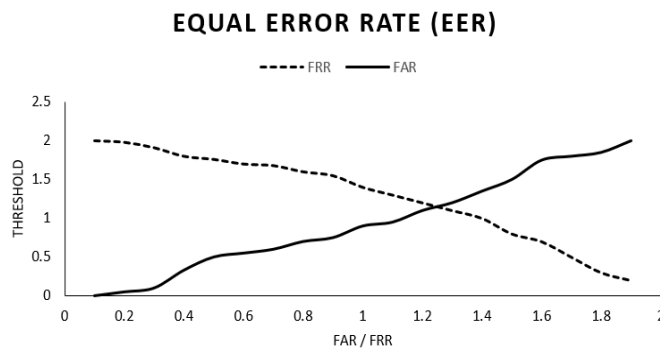


Figure 12. EER of the system

**4.1. Comparison of performance**

The comparison of the accuracy of the segmentation algorithm is presented in Table 3. The segmentation algorithm proposed in this document achieved an accuracy of 99.9% using the SBVPI eye image database. The segmentation accuracy recorded for the manually captured eye images was 100%. This accuracy shows a higher performance without the required training for deep learning techniques when compared with the closest method in Table 3. A close look at the comparison of the system’s segmentation performance is shown in Table 4.

Table 3. Segmentation accuracy comparison table

Paper	Method	Accuracy (%)	
Rot <i>et al.</i> [1]	Saviola method	SBVPI	98.1
Dong <i>et al.</i> [30]	Otsu thresholding	UBIRIS v1	98.1
Pathak <i>et al.</i> [3]	CNN	MMU	98
		UBIRIS v2	99.423
This study	Circular hough and modified run-data based following algorithm	SBVPI	99.9
		Manual capture	100

Table 4. Comparison of the proposed system performance with other systems

Paper	Accuracy (%)
Pathak <i>et al.</i> [3]	97.99
Maheshan <i>et al.</i> [7]	87.65
Proposed	99.98 (SBVPI)
	99.99 (Captured database)

## 5. CONCLUSION

The advent of biometric traits for solving security challenges has been an area of much research. More traits are being discovered, amongst which is the sclera. However, the segmentation of the sclera in an eye image has been an area that requires more accuracy. This study has proposed an approach for the segmentation of the sclera. The approach uses circular hough transform and a modified run-data based algorithm. The accuracy of the presented segmentation algorithm showed an improvement when compared with previous approaches. This sclera segmentation technique is robust as it allows for the extraction of sclera on both sides of the iris. The proposed algorithm also made use of circular hough transform to recognize the iris. This can make the segmentation of both the sclera and the iris seamless. It also requires less computation resource and no training when compared to supervised learning-based techniques. The paper presented a sclera system using the proposed segmentation technique and compound local binary pattern. The system showed an encouraging performance.

## ACKNOWLEDGEMENTS

Authors appreciate Landmark University Centre for Research and Development, Landmark University, Omu-aran, Nigeria for fully sponsoring the publication of this research article.




## REFERENCES

- [1] P. Rot, M. Vitek, K. Grm, Ž. Emeršič, P. Peer, and V. Štruc, "Deep Sclera Segmentation and Recognition," *Advances in Computer Vision and Pattern Recognition*, pp. 395–432, 2020, doi: 10.1007/978-3-030-27731-4\_13.
- [2] D. Xu, W. Dong, and H. Zhou, "Sclera Recognition Based on Efficient Sclera Segmentation and Significant Vessel Matching," *Computer Journal*, vol. 65, no. 2, pp. 371–381, 2022, doi: 10.1093/comjnl/bxaa051.
- [3] M. Pathak, N. Srinivasu, and V. Bairagi, "Effective segmentation of sclera, iris and pupil in noisy eye images," *Telecommunication Computing Electronics and Control*, vol. 17, no. 5, pp. 2346–2354, 2019, doi: 10.12928/TELKOMNIKA.v17i5.12551.
- [4] M. S. Maheshan, B. S. Harish, and S. V. A. Kumar, "Sclera Segmentation using Spatial Kernel Fuzzy Clustering Methods," in *International Conference on Pattern Recognition Applications and Methods*, SCITEPRESS-Science and Technology Publications, 2020, pp. 433–439, doi: 10.5220/0008935704330439.
- [5] M. Vitek, P. Rot, V. Štruc, and P. Peer, "A comprehensive investigation into sclera biometrics: a novel dataset and performance study," *Neural Computing and Applications*, vol. 32, no. 24, pp. 17941–17955, 2020, doi: 10.1007/s00521-020-04782-1.
- [6] M. K. Pathak, N. Srinivasu, and V. Bairagi, "Support value based fusion matching using iris and sclera features for person authentication in unconstrained environment," *Journal of Engineering Science and Technology*, vol. 15, no. 4, pp. 2595–2609, 2020.
- [7] M. S. Maheshan, B. S. Harish, and N. Nagadarshan, "A convolution neural network engine for sclera recognition," *International Journal of Interactive Multimedia and Artificial Intelligence*, vol. 6, no. 1, pp. 78–83, 2020, doi: 10.9781/ijimai.2019.03.006.
- [8] S. Lee and J. Kim, "A bifurcation-based descriptor for sclera recognition," *ICEIC 2019-International Conference on Electronics, Information, and Communication*, pp. 1–3, 2019, doi: 10.23919/ELINFOCOM.2019.8706438.
- [9] D. Zhu, J. Li, H. Li, J. Peng, X. Wang, and X. Zhang, "A Less-constrained Sclera Recognition Method based on Stem-and-leaf Branches Network," *Pattern Recognition Letters*, vol. 145, pp. 43–49, 2021, doi: 10.1016/j.patrec.2021.01.025.
- [10] L. H. Gong, C. Tian, W. P. Zou, and N. R. Zhou, "Robust and imperceptible watermarking scheme based on Canny edge detection and SVD in the contourlet domain," *Multimedia Tools and Applications*, vol. 80, no. 1, pp. 439–461, 2021, doi: 10.1007/s11042-020-09677-w.
- [11] X. Hu and Y. Wang, "Monitoring coastline variations in the Pearl River Estuary from 1978 to 2018 by integrating Canny edge detection and Otsu methods using long time series Landsat dataset," *Catena*, vol. 209, no. P2, p. 105840, 2022, doi: 10.1016/j.catena.2021.105840.
- [12] Erwin and T. Yuningsih, "Detection of Blood Vessels in Optic Disc with Maximum Principal Curvature and Wolf Thresholding Algorithms for Vessel Segmentation and Prewitt Edge Detection and Circular Hough Transform for Optic Disc Detection," *Iranian Journal of Science and Technology - Transactions of Electrical Engineering*, vol. 45, no. 2, pp. 435–446, 2021, doi: 10.1007/s40998-020-00367-9.
- [13] S. Nanayakkara, "A Review of Literature on Iris Recognition," *International Journal of Research*, vol. 9, no. 2, p. 106, 2020, doi: 10.32968/1632-2882.
- [14] B. Aisha *et al.*, "Hardware Synthesize and Performance Analysis of Intelligent Transportation Using Canny Edge Detection Algorithm," *International Journal of Engineering and Manufacturing*, vol. 11, no. 4, pp. 22–32, 2021, doi: 10.5815/ijem.2021.04.03.
- [15] F. Wu, C. Zhu, J. Xu, M. W. Bhatt, and A. Sharma, "Research on image text recognition based on canny edge detection algorithm and k-means algorithm," *International Journal of System Assurance Engineering and Management*, vol. 13, no. S1, pp. 72–80, 2022, doi: 10.1007/s13198-021-01262-0.
- [16] W. Lu, B. Xie, and Z. Ding, "Edge Detection Algorithm-Based Lung Ultrasound in Evaluation of Efficacy of High-Flow Oxygen Therapy on Critical Lung Injury," *Computational and Mathematical Methods in Medicine*, vol. 2022, 2022, doi: 10.1155/2022/3604012.




- [17] L. Z. L. Huihui, Y. Kun, Z. Lixuan, L. Wei, "Circular Pointer Instrument Recognition System based on MobileNetV2," *Journal of Computers and Applications*, vol. 41, no. 4, pp. 1214–1220, 2021.
- [18] C. W. Chuang and C. P. Fan, "Deep-learning based joint iris and sclera recognition with yolo network for identity identification," *Journal of Advances in Information Technology*, vol. 12, no. 1, pp. 60–65, 2021, doi: 10.12720/jait.12.1.60-65.
- [19] S. D. Salehi, W. Gilliland, and O. T. Kingstedt, "Application of the Hough Transform for Automated Analysis of Kolsky Bar Data," *Experimental Techniques*, vol. 46, no. 1, pp. 153–165, 2022, doi: 10.1007/s40799-021-00458-0.
- [20] F. Suvari, "Image processing based drape measurement of fabrics using circular Hough transformation," *Journal of the Textile Institute*, vol. 112, no. 5, pp. 846–854, 2021, doi: 10.1080/00405000.2020.1782553.
- [21] Y. Zhuang, X. Zhao, Z. Huang, L. Han, K. Chen, and J. Lin, "AutoCellANLS: An Automated Analysis System for Mycobacteria-Infected Cells Based on Unstained Micrograph," *Biomolecules*, vol. 12, no. 2, pp. 1–17, 2022, doi: 10.3390/biom12020240.
- [22] Y. Yang, J. Wang, and Y. Xue, "Iris boundary localization based on Hough transform and the quadratic circle data compensation," *International Journal of Imaging Systems and Technology*, vol. 31, no. 3, pp. 1357–1365, 2021, doi: 10.1002/ima.22535.
- [23] J. Seo, S. Chae, J. Shim, D. Kim, C. Cheong, and T. D. Han, "Fast contour-tracing algorithm based on a pixel-following method for image sensors," *Sensors (Switzerland)*, vol. 16, no. 3, pp. 1–27, 2016, doi: 10.3390/s16030353.
- [24] S. Karanwal, "A comparative study of 14 state of art descriptors for face recognition," *Multimedia Tools and Applications*, vol. 80, no. 8, pp. 12195–12234, 2021, doi: 10.1007/s11042-020-09833-2.
- [25] N. Mishra and A. Bhatt, "Feature extraction techniques in facial expression recognition," in *Proceedings-5th International Conference on Intelligent Computing and Control Systems*, IEEE, pp. 1247–1251, 2021, doi: 10.1109/ICICCS51141.2021.9432192.
- [26] K. Shang, H. Ishibuchi, and Y. Nan, "Distance-based subset selection revisited," *GECCO 2021 - Proceedings of the 2021 Genetic and Evolutionary Computation Conference*, no. 1, pp. 439–447, 2021, doi: 10.1145/3449639.3459391.
- [27] A. Elen and E. Avuçlu, "Standardized Variable Distances: A distance-based machine learning method," *Applied Soft Computing*, vol. 98, p. 106855, 2021, doi: 10.1016/j.asoc.2020.106855.
- [28] C. S. Hong and T. G. Oh, "TPR-TNR plot for confusion matrix," *Communications for Statistical Applications and Methods*, vol. 28, no. 2, pp. 161–169, 2021, doi: 10.29220/CSAM.2021.28.2.161.
- [29] S. Das, I. De Ghosh, and A. Chattopadhyay, "An efficient deep sclera recognition framework with novel sclera segmentation, vessel extraction and gaze detection," *Signal Processing: Image Communication*, vol. 97, p. 116349, 2021, doi: 10.1016/j.image.2021.116349.
- [30] W. Dong, H. Zhou, and D. Xu, "A New Sclera Segmentation and Vessels Extraction Method for Sclera Recognition," *2018 10th International Conference on Communication Software and Networks*, pp. 552–556, 2018, doi: 10.1109/ICCSN.2018.8488229.

## BIOGRAPHIES OF AUTHORS






**Tunde Taiwo Adeniyi**    received his Bachelor degree in Computer Science from Adamawa State University, Adamawa, Nigeria. He holds an M.Tech. in Computer Science from Federal University of Technology, Akure, Nigeria. He is currently working towards a Doctoral degree in the Department of Computer Science, University of Ilorin, Ilorin, Nigeria. His interest includes various areas such as biometrics, computer vision, security, artificial intelligence, and machine learning. He can be contacted at email: adekitos2@gmail.com.



**Oladele Tinuke Omolewa**    is a Senior lecturer in the Department of Computer Science, Faculty of Communication and Information Sciences, University of Ilorin, Ilorin, Nigeria. She obtained her B.Sc. in Computer Science from the University of Benin, Benin City, Edo State. She bagged her M.Sc. in Mathematics (Computer Science Option) from the University of Ilorin and a Ph.D. in Computer Science also from the University of Ilorin. She is currently an Associate Professor at the University of Ilorin. She is known across board for her innovative research work in Bioinformatics and Computational Biology. Her research interest includes artificial intelligence, data mining, and cyber security. She can be contacted at email: Oladele.to@unilorin.edu.ng.



**Jide Kehinde Adeniyi**    received his Bachelor degree in Computer Science from Adamawa State University, Adamawa, Nigeria. He holds an M.Tech. in Computer Science from Federal University of Technology, Akure, Nigeria. He obtained his doctoral degree in the Department of Computer Science, University of Ilorin, Ilorin, Nigeria. His interest includes various areas such as biometrics, computer vision, security, artificial intelligence, and machine learning. He can be contacted at email: adeniyi.jide@lmu.edu.ng.